RSC Advances

ROYAL SOCIETY OF CHEMISTRY

www.rsc.org/advances

Graphical abstract

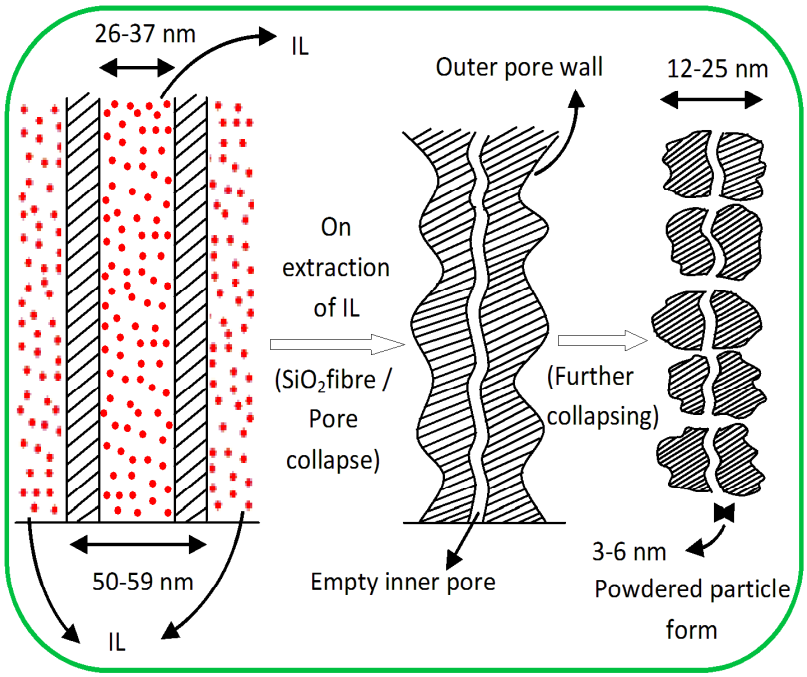

Ionic Liquid template assisted synthesis of porous nano-silica nails

Yogendra Lal Verma[a], Rajendra Kumar Singh[a]*, Il-Kwon Oh[b] and Suresh Chandra

Abstract

The strategy planned to obtain porous materials was to synthesize porous silica at a fast gelation rate which can be attained by using non-hydrolytic sol-gel route with high ionic liquid (IL) – loading. Then the silica might get drawn into a tubular spring-like structure that would cage the ionic liquid within its fold and that some ionic liquid might get into the pores of the silica spring. To test this strategy, we used a mixture of tetra methyl ortho-silane and ionic liquid in such a ratio that the resulting product, SiO_2: IL, has a content of IL as high as 85-92 wt%. Interestingly, the experimental results described in this paper have proved the validity of our strategy to obtain "porous" nano-silica particles (sometimes, "porous nail" structures also resulted).

Keywords: Ionic liquid, Porous materials, Sol-gel process, Confinement

---

[a] Department of Physics, Banaras Hindu University, Varanasi 221005, India, Fax: (+91) 542 2368390; Tel:(+91) 542 6701541;
[*] E-mail: rksingh_17@rediffmail.com,
[b] School of Mechanical, Aerospace and Systems Engineering, Korea Advanced Institute of Science and Technology (KAIST), 291 Daehak-ro, Yuseong-gu, Daejeon 305-701, Republic of Korea, E-mail: ikoh@kaist.ac.kr

Introduction

Porous nano-silica particles or nano-tubes have found many applications, particularly in the formation of a wide variety of nano-composites[1-2]. The pores of such materials can be filled with some drug (to be used for drug delivery[3]), other bioactive materials for bio-sensing[4], catalytic reagents[5], etc. With the recent discovery of ionic liquids (composed of organic cations and inorganic / organic anions)[6-8], a sudden burst of activity has started in order to develop solid state ionic materials based on ionic liquids, *e.g.* ionic liquid modified polymers[9] and ionic liquid filled porous membranes[10-11] (called "ionogels") for electrochemical devices applications[12-17]. The first ionogel was developed by Dai *et al.*[18], in an ionic liquid incorporated in porous silica; however, earlier, Srivastava & Chandra[19] reported material in which an ionic salt solution was incorporated in porous silica.

Since the work of Dai *et al.*[18] many reports have become available for porous silica filled with ionic liquid, obtained by hydrolytic and non-hydrolytic routes[20-22]. All these studies were focused on ionogel ingots with low amounts of IL; and, the ionic liquid was acting as a porous structure directing the template. These ionogels had high ionic conductivity. In our earlier studies, lower wt% ILs (in the range of 10-68 wt %) were impregnated in silica[23-27] and TiO_2 matrices[28] by using hydrolytic and non-hydrolytic sol-gel processes. Changes in various physicochemical parameters such as phase transition temperatures (glass transition[23,25-28], crystallization and melting temperatures[23,25,27]), dielectric relaxation behaviour[29], optical properties[23-28] etc. of ionic liquids were reported by us in these ionogels upon confinement in porous matrices. Recently, few studies are reported on immobilization of high amount of ILs using hydrolytic and non-hydrolytic methods[30-33]. Noor et al.[32] and Horowitz et al.[33] did try to immobilize high ionic liquid content (as high as ≤ 97 %) in a silica matrix. They succeeded in

obtaining a high conductivity comparable to that of a pure ionic liquid. Present study incorporating IL upto 92 wt% resulted monolith with mechanical integrity. As hypothesized in the introductory paragraph, the present paper is focused on optimizing the conditions for obtaining silica monoliths (from the sol-gel non-hydrolytic route) with high content of ionic liquid.

The questions addressed are: (i) How can a small amount of silica immobilize within its fold a large amount of ionic liquid? Can this be modelled? (ii) Does the modelled mechanism lead to special structural features? Can this be observed experimentally? We report the formation of porous nano-silica nails and nano particles of silica using sol-gel synthesis. (iii) How do the properties of an immobilized ionic liquid change? Is there some evidence of silica-ionic liquid interaction?

Experimental Section

The chemicals used in this study were: Tetramethyl orthosilicate (TMOS), and ionic liquid 1-ethyl-3-methylimidazolium thiocyanate ([EMIM][SCN]) purchased from Sigma Aldrich. Before use, the IL was heated to 100 °C and vacuum dried at a pressure of 10^{-6} Torr for 12 hours to remove traces of water. Formic acid (GR Grade) was purchased from Merck Germany and used as received.

In the synthesis of the ionic liquid assisted porous silica nano-nails, non hydrolytic sol-gel process[25,34] has been used. Ionic liquid and formic acid were taken in a reaction vessel and mixed properly before adding tetramethyl orthosilicate (TMOS). The molar ratio of TMOS & formic acid (n_{TMOS} : n_{IL}) was 1:8 and ionic liquid molar ratios were chosen in such as a way that resulting product SiO_2 : IL has IL content as high as 85- 92 wt%. It may be remarked that on completion of gelation process, one mole of TMOS yields one mole of SiO_2. After mixing IL,

formic acid and TMOS; sol-gel reaction was completed at ambient temperature and pressure. The complete sol-gel reaction (corboxilation, estrification, hydrolysis and condensation) is given by equation 1.

$$(CH_3O)Si + 2HC(O)OH \longrightarrow SiO_2 + 2CH_3OH + 2HC(O)OCH_3 \quad \text{..... (1)}$$

Gelation occurred within 3-6 h. The aging process was followed by measuring the weight at different times. The aging was considered to have been accomplished, after which no more weight loss was noticeable. The aging time was ~15 days. The samples prepared with ionic liquid loadings 85 wt%, 90 wt% and 92 wt% are referred as SG-IL85, SG-IL 90 and SG-IL92 respectively. Photographs of stable monoliths (after cutting in rectangular shapes) of samples SG-IL90 and SG-IL92 are shown in Fig. 1.

Surface morphological investigations of the samples were performed using a scanning electron microscope (SEM) Magellan 400. The TEM image was recorded on Tecnai G2F30. N_2- sorption measurement were carried out using a Gemini VII 2390t, from the Micromeritics Instrument Corporation, at 77 K. Prior to N_2-sorption measurements, ionogels were washed with deionised water more than 5 times for extracting the ionic liquid. IL extracted samples were dried at 100 ˚C for 12 h to remove the water content and then degassed at 60 ˚C for 15 h under vacuum. Before the analysis, samples were degassed under N_2 flow at 60 ˚C for 24 h. After extraction of ionic liquids, samples: SG-IL85, SG-IL 90 and SG-IL92 are denoted as WSG-IL85, WSG-IL 90 and WSG-IL92 respectively**.** DSC measurement was used to characterise the thermal transition in the bulk IL and confined IL. Measurements were performed using a Mettler Toledo DSC-1 at a scanning rate of 10 ˚C per minute in a nitrogen environment. The thermogravimetric analysis was carried out with Mettler Toledo TGA / DSC 1 analyser and data were evaluated with Stare software. All the samples were run in alumina

(Al_2O_3) pan at heating rate 10°C min under N_2 atmosphere. Fluorescence spectra were recorded at room temperature with a Perkin Elmer LS 45 Fluorescence Spectrometer with a pulsed xenon lamp as excitation source and a photomultiplier tube as detector. The FTIR spectra were recorded using a Perkin Elmer spectrum 65 FTIR spectrometer.

Result and Discussion

Let us address the first two questions for holding such a large amount of ionic liquid. The silica matrix is expected to be a mesh-like coiled network of silica nano-nails, as schematically illustrated in Fig. 2. The expected surface morphological features can be seen clearly in Fig. 2a-c. Fig. 2a and 2b show that protruded straight or bent nano-rod shells appear. If these nano-nails break at the surface, then the visible feature will be an "array" of nano-heads of silica. Most of the ionic liquid will be caged in the mesh; a part of the ionic liquid may get into the pores of the main body of the nano-spring. SEM images of our synthesized ingots are shown in Fig. 3, which interestingly shows the presence of these modelled morphologies.

Fig. 3a and 3b correspond to different regions of the sample containing 85 wt % IL (SG-IL85), in which we can see porous silica-nano nails protruding from the surface, as modelled in Fig. 2b and 2c earlier. Similar morphological features can be seen in Fig. 3c and 3d for the silica gel sample containing 90 wt% of IL (SG-IL90).

The silica structural features of SG-IL90 are more ordered than those of SG-IL85. Some regions of the SG-IL90 and SG-IL85 surfaces appear as shown in Fig. 3e-f and 3g, respectively. This resembles the modelled surface (see Fig. 2a). The outer diameters of the silica spring nano-nails are of the order of 50-58 nm; the inner diameter is of the order of 26-34 nm. As an illustrative example, these diameters are specified in Fig. 3d and 3f. The results discussed above show a successful synthesis of porous nano-nails or nano-rods.

Fig. 4a shows a typical SEM image of WSG-IL85 (after extracting the IL from SG-IL85). The SEM image reveals the nano-particles to have different sizes. The particle sizes are calculated from the SEM image (Fig. 4a) and are illustrated by the histogram (shown in the inset of Fig. 4a). From the histogram, it can be seen that most of the particles have sizes ranging between 20 and 25 nm. To show that after the extraction of IL from porous silica the nano-nails are formed into porous silica nano-particles, we have modelled a mechanism of the formation of the porous silica nano-particles shown in Fig. 4b. This figure illustrates that due to the extraction of IL from the pores and outside the porous nano-silica rod, (i) the pore collapses and (ii) further collapse results in the formation of porous-SiO_2 particles. Because of this, and due to the low resolution of the SEM and the smaller pore size of the porous silica nano-particles, pores are not observed in SEM image (Fig. 4a).

To elucidate the porous structure of the silica-nano particles (which has been modelled by us as shown in Fig. 4b), we have characterized the IL extracted sample by N_2-sorption measurement and TEM study. Fig. 4c shows typical N_2-sorption isotherms and pore size distribution curves for WSG-IL-85, WSG-IL90, and WSG-IL92. These isotherms show themselves to be type-IV N_2-sorption isotherms with large hysteresis, indicating 3D interconnected mesoporous structure[35]. Pore size distribution curves obtained using the Barrett-Joyner-Halenda (BJH) method show a uniform pore size distribution. Pore parameters of all the samples are given in Table 1. From the Table 1, it can be seen that sample WSG-IL85 has highest surface area (578 m^2/g), pore volume (~0.71 cm^3/g) and pore size (~ 4 nm) as compared to the samples WSG-IL90 and WSG-IL92. A distinctive TEM micrograph of WSG-IL85 after extraction of IL (see Fig. 4d) also confirms that the silica nano-particles are porous, having pore sizes of the order of 3-6 nm, *i.e.*, average pore size obtained from the N_2-sorption measurement

matches the pore size obtained in the TEM micrograph. Thus, TEM micrograph and N_2-sorption measurement confirm the porous texture of the silica nano-particles obtained after extracting the ionic liquid. Our modelled schematic presentation supports the morphological characterization well. So far, we have discussed the morphology of SiO_2 ingot/ porous nano-silica nails. Now we address the third question of interest, *i.e.* how the properties of IL change in confinement.

To describe the properties of IL in confinement, we have characterised our samples using differential scanning calorimetry (DSC), fluorescence spectroscopy and Fourier transform infrared spectroscopy (FTIR).To investigate the thermal phase transition behaviour of ionic liquids upon confinement, DSC measurement has been carried out. Fig. 5 shows the DSC thermograms of bulk IL and confined IL (SG-IL85, SG-IL90 & SG-IL92). From the DSC thermograms shown in Fig. 5, it has been observed that pure and confined IL show only the glass transition temperature (T_g). It can be seen that T_g of bulk IL has increased ~ 4-6 ˚C in comparison to bulk IL. Gobel et al.[31] also reported the increase in glass transition temperature (~1˚C) of IL ([EMIM][SCN])upon confinement in silica matrix. This change in the glass transition temperature of confined IL may be due to silica pore wall surface interaction with IL molecules as discussed in FTIR section.

Thermogravimetric analysis (shown in Fig. 6) has been used to determine the thermal stability of bulk ionic liquid ([EMIM][SCN]) and confined IL (SG-IL85, SG-IL90 & SG-IL92). From the TGA thermograms, it can be seen that a small initial weight loss has been observed in the temperature range 35˚C to 120˚C due to the remaining organic solvents and physically absorbed water (absorbed during synthesis process and in handling the sample for TGA measurement). TGA curves of bulk and confined IL show single step decomposition with their onset decomposition temperature, T_d ~225˚C indicating good thermal stability. From TGA

curves it can clearly be seen that the residues of the samples (SG-IL85, SG-IL90 and SG-IL92) after complete decomposition (at 500˚C) are approximately equal to the weight % of silica in samples; i.e. ~ 15, 10 and 8 wt% for SG-IL85, SG-IL90 and SG-IL92 respectively. Inset of Fig. 6 shows the TGA thermograms of a typical ionogel (SG-IL90) after extraction of ionic liquid (referred as WSG-IL90) and pure SiO_2. The inset TGA curves show that thermograms of WSG-IL90 and pure SiO_2 are alike. In these thermograms (inset), weight loss is occurring due to the evaporation of water and breaking of OH groups present on the surface of silica pore wall surface[36].

The properties of IL upon confinement have also been examined using fluorescence spectroscopy. The fluorescence emission spectra of bulk IL ([EMIM][SCN]) and the IL confined silica gel matrix (SG-IL85) are shown in Fig. 7a and 7b. Here, the fluorescence emission spectra have been found to be independent of the excitation wavelength for bulk IL as well as for confined IL (SG-IL85). Bulk IL exhibits a broad fluorescence emission at 525 nm while, upon confinement, three fluorescence emission peaks at 440 nm, 530 nm, and ~ 575 nm have been observed. The emission observed at 440 nm is because of the SiO_2 matrix; the other emissions are IL-related. The peak appearing at 530 nm is approximately the same as that of the bulk sample. The peak observed at 575 nm could be due to ionic liquid trapped in the pores of porous nano-silica nails, which would lead to red shift due to the liquid's interaction with the pore wall surface. Overall, the properties of IL have been found to change upon confinement.

FTIR study has been carried out to observe the interaction of IL molecules with the silica pore wall surface. FTIR spectra of bulk and confined IL are shown in Fig. 8a while Fig. 8b shows the region of those vibrational bands in which changes have been observed. From the Fig. 8b, it can be seen that the vibrational bands of pure IL ([EMIM][SCN]) observed at 3156

cm^{-1} and 3114 cm^{-1} are attributed to asymmetric stretching of HCCH and CH and the stretching of the NC(H)N of the imidazolium ring, respectively [37-38]. These vibrational bands of pure IL show a change of ~ 3-6 cm^{-1} upon confinement (shown in Fig. 8b). Changes observed in the vibrational bands and phase transition temperatures of ionic liquid upon confinement have been explained on the basis of interaction of IL and silica pore wall surface[23-25, 36, 39]. In our previous studies, we have also reported the interaction of silica pore wall surface with ionic liquids ([BMIM][$OcSO_4$][23], [EMIM][$EtSO_4$][36] and [EMIM][SCN])[37] theoretically by DFT calculation after optimizing the structure of IL cation and anion pair in bulk and confinement (using Gaussian 03 package). The interaction between silica pore wall surface and IL ([EMIM][SCN]) has also been shown by us using DFT calculation[37]. From this study[37], it has been found that oxygen and OH groups (hydrolysed silica; in which unintentional and unavoidable OH groups are present on the surface) present on the silica pore wall surface interact with C-H of the cation ring and anion (SCN^-) of the IL respectively. Similarly, in the present study, changes in the vibrational bands related to C-H of cation of IL ring may also be due to the interaction of C-H of IL ring with Si-O-Si and OH-Si of silica pore wall. Changes (~1-3 cm^{-1}) in the IL anion SCN^- related vibrational band (at 2059 cm^{-1})[38] has also been observed which is attributed to the H-bonding between hydroxyl group at the silica pore wall surface and nitrogen of the IL anion[39-40].

Conclusions

In the present work, we have demonstrated a design strategy in which a silica sol-gel precursor guided higher IL immobilisation. Our design allowed for high IL loadings up to 92 wt%. We present a modelled mechanism for the immobilisation of such a high amount of IL in a small

amount of silica. Pores of the porous silica ingot produced using the non-hydrolytic sol-gel process were filled with IL. The results from a scanning electron microscopy assay of the as synthesized samples (SG-IL85 and SG-IL90) show that the silica gel has a tubular spring-like structure caging the ionic liquid within its fold, with some ionic liquid trapped in the pores of the silica spring, which is as per our design strategy. Further, after the removal of IL from the samples, the resulting porous silica nano-particles were characterised by BET and TEM analysis. The formation of silica nano-particles after the extraction of IL from tubular silica nails has also been modelled by us. The properties of IL (e.g. glass transition temperature, vibrational bands related to ring of IL, and fluorescence properties) have been found to change due to the interaction of IL with the silica pore wall surface. Our findings could lead to the use of tubular porous silica nails and porous nano silica in fields such as drug delivery, biosensing, catalytic reagents, etc.

Acknowledgements

RKS is grateful to the Department of Science & Technology, New Delhi, and Board of Research in Nuclear Sciences (2013/34/14/BRNS)-DAE, India, for providing financial assistance for carrying out this work, YLV is thankful to Council of Scientific and Industrial Research, New Delhi, India, for award of Senior Research Fellowship (SRF).

References

1. P. Wang, S. M. Zakeeruddin, P. Comte, I. Exnar, M. Gratzel, *J. Am. Chem. Soc.*, 2003,125, 1166.
2. T. Torimoto, T. Tsuda, K. Okazaki, S. Kuwabata, *Adv. Mater.*, 2010, 22, 1196.

3. M. Vallet-Regí, F. Balas, D. Arcos, *Angew. Chem. Int. Ed.*, 2007, 46, 7548.

4. Y. Liu, Y. Liu, L. Shi, M. Wang, Z. Li, H. Liua, J. Li, *Green Chem.*, 2005, 7, 655.

5. A. Taguchi, F. Schuth, *Micropor. Mesopor. Mater.*, 2005, 77, 1.

6. F. Endres, D. MacFarlane, A. Abbott, (Eds.), Electrodeposition from Ionic Liquids, Wiley-VCH, 2008.

7. M. Armand, F. Endres, D. R. MacFarlane, H. Ohno, B. Scrosati, *Nature Mater.*, 2009, 8, 621.

8. J. P. Hallett, T. Welton, *Chem. Rev.*, 2011, 111, 3508.

9. J. Lu, F. Yan, J. Texter, *Prog. Polym. Sci.*, 2009, 34, 431.

10. A. P. De los Rios, F. J. Hernandez-Fernandez, F. Tomas-Alonso, J. M. Palacios, D. Gomez, M. Rubio, G. Vıllora, *J. Membr. Sci.*, 2007, 300, 88.

11. F. Gayet, L. Viau, F. Leroux, S. Monge, J. J. Robin, A. Vioux *J. Mater. Chem.*, 2010, 20, 9456.

12. S. Ito, S. M. Zakeeruddin, P. Comte, P. Liska, D. Kuang, M. Gratzel, *Nature Photon.*, 2008, 2, 693.

13. A. Balducci, F. Soavi, M. Mastragostino, *Appl. Phys. A*, 2006, 82,627.

14. J. Le Bideau, L. Viau, A. Vioux, *Chem. Soc. Rev.*, 2011, 40, 907-925.

15. T. Katakabe, T. Kaneko, M. Watanabe, T. Fukushima, T. Aida, J. *Electrochem. Soc.*, 2005, 152, A1913.

16. S. Y. Chew, J. Sun, J. Wang, H. Liu, M. Forsyth, D. R. MacFarlane, *Electrochim. Acta.*, 2008, 53, 6460.

17. M. P. Singh, R. K. Singh, S. Chandra, *Prog. Mater. Sci.*, 2014, 64, 73–120.

18. S. Dai, Y. H. Ju, H. J. Gao, J. S. Lin, S. J. Pennycook, C. E. Barnes, *Chem. Commun.*, 2010, 243.

19. R. Srivastava, S. Chandra, *Phys. Status Solidi (a)*, 2002, 191, 202.

20. A. Vioux, L. Viau, S. Volland, J. Le Bideau, *C. R. Chimie*, 2010, 13, 242.

21. J. Le Bideau, M. Y. Miah, A. Vioux, F. Fajula, A. Galarneau, *J. Mater. Chem*., 2010, 20, 964.

22. L. Viau, M.-A. Neouze, C. Biolley, S. Volland, D. Brevet, P. Gaveau, P. Dieudonne, A. Galarneau, A. Vioux, *Chem. Mater.*, 2012, 24, 3128

23. M. P. Singh, R. K. Singh, S. Chandra, *J. Phys. Chem. B*, 2011, 115, 7505.

24. M. P. Singh, R. K. Singh, S. Chandra, *ChemPhysChem*, 2010, 11, 1.

25. A. K. Gupta, M. P. Singh, R. K. Singh, S. Chandra, *Dalton Trans.*, 2012, 41, 6263.

26. Y. L. Verma, M. P. Singh, R. K. Singh, *J. Nanomater*., 2012, 2012, 1.

27. A. K. Gupta, R. K. Singh, S. Chandra, *RSC Adv.*, 2013, 3, 13869.

28. Y. L. Verma, M. P. Singh, R. K. Singh, *Mater. Lett.*, 2012, 86, 73.

29. M. P. Singh, Y. L. Verma, A. K. Gupta, R. K. Singh, S. Chandra, *Ionics*, 2014, 20, 507.

30. M.-A. Neouze J. Le Bideau, F. Leroux, A. Vioux, *Chem. Commun.*, 2005, 1082.

31. R. Gobel, P. Hesemann, J. Weber, E. Moller, A. Friedrich, S. Beuermann, A. Taubert, *Phys.Chem.Chem.Phys.*, 2009,11, 3653.

32. S. A. M. Noor, P. M. Bayley, M. Forsyth, D. R. MacFarlane, *Electrochim. Acta.*, 2013, 91, 219.

33. A. I. Horowitz, M. J. Panzer, *J. Mater. Chem.*, 2012, 22, 16534.

34. K. G. Sharp, *J. Sol-Gel Sci. Techn.*, 1994, 2, 35.

35. K. S. W. Sing, D. H. Everett, R. A. W. Haul, L. Moscou, R. A. Pierotti, J. Rouquerol T. Siemieniewska, *Pure & Appl. Chem.*, 1985, 57, 603.

36. A. K. Gupta, Y. L. Verma, R. K. Singh, S. Chandra, *J. Phys. Chem. C*, 2014, 118, 1530.

37. Y. L. Verma, A. K. Gupta, R. K. Singh, S. Chandra, *Micropor. Mesopor. Mater.*, 2014, 195, 143.

38. E. R. Talaty, S. Raja, V. J. Storhaug, A. Do1lle, W. R. Carper, *J. Phys. Chem. B*, 2004, 108, 13177.

39. Y. Liu, G. Wu, H. Fu, Z. Jiang, S. Chen, M. Sha, *Dalton Trans.*, 2010, 39, 3190.

40. B. D. Fitchett, J. C. Conboy, *J. Phys. Chem. B*, 2004, 108, 20255.

Table 1. Pore parameters of samples (SG-IL85, SG-IL90 and SG-IL92) after extracting the IL.

Samples	BET surface area (m^2/g)	Total pore volume (cm^3/g)	Average pore diameter (nm)
SG-IL85	578	0.71	3.95
SG-IL90	472	0.52	3.46
SG-IL92	486	0.59	3.76

Figure Captions

Fig. 1 Photographs of stable monoliths of samples SG-IL90 and SG-IL92 after cutting in rectangular shape.

Fig. 2 Schematic diagram (model) illustrating the morphology of formation of porous nano-

silica nails. (a) Representation of the model for formation of SiO_2 spring-like mesh matrix which holds or immobilizes or cages the ionic liquid within its fold and which shows the nano-porous silica heads at the upper surface. (b) Small porous nano-rods emerging out from the surface. (c) Bent porous nano-rods at the surface.

Fig. 3 SEM images of IL-template assisted tubular porous-nano silica nails are shown in Fig. (a), (b) & (g) for SG-IL85 and (c) - (f) for SG-IL90. Inset of Fig. (d) shows the extended view of tubular porous nano-rods in the corresponding SEM image and inset of Fig. (e) shows the extended view of dotted circular space.

Fig. 4 Textural characterization of porous nano silica nano particles. (a) SEM image of porous nano silica after extracting the ionic liquid from the sample SG-IL-85. Inset of Fig. (a) gives the histogram of the particles size distribution observed from the SEM image. (b) Schematic representation of formation of porous silica nano-particle after extraction of IL. (c) Pore size distributions of SG-IL85, SG-IL90 and SG-IL92 with inset showing corresponding Nitrogen adsorption-desorption isotherms. Pore size distributions were calculated based on the BJH method using the adsorption isotherm. (d) TEM image of the sample SG-IL-85 after extracting the ionic liquid.

Fig. 5 Glass transition temperature (T_g) of bulk and immobilized IL into the porous nano silica nails (IL-85, IL-90 and IL-92).

Fig. 6 TGA thermograms of bulk IL ([EMIM][SCN]) and IL confined silica gels (SG-IL85, SG-IL90 and SG-IL92). Inset shows the TGA thermogram of a typical ionogel (SG-IL90) after extraction of ionic liquid termed as WSG-IL90 and pure SiO_2.

Fig. 7 Fluorescence emission spectra of (a) bulk IL and (b) confined IL (SG-IL85).

Fig. 8 FTIR spectra of (a) bulk IL and confined IL samples (SG-IL85, SG-IL90 and SG-IL92)

and their (b) extended region 3050-3200 cm^{-1} in which the C-H vibration of IL cation ring lies.

Fig. 1.

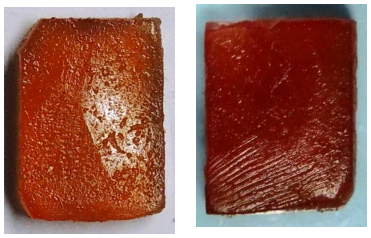

SG-IL90 **SG-IL92**

Fig. 2.

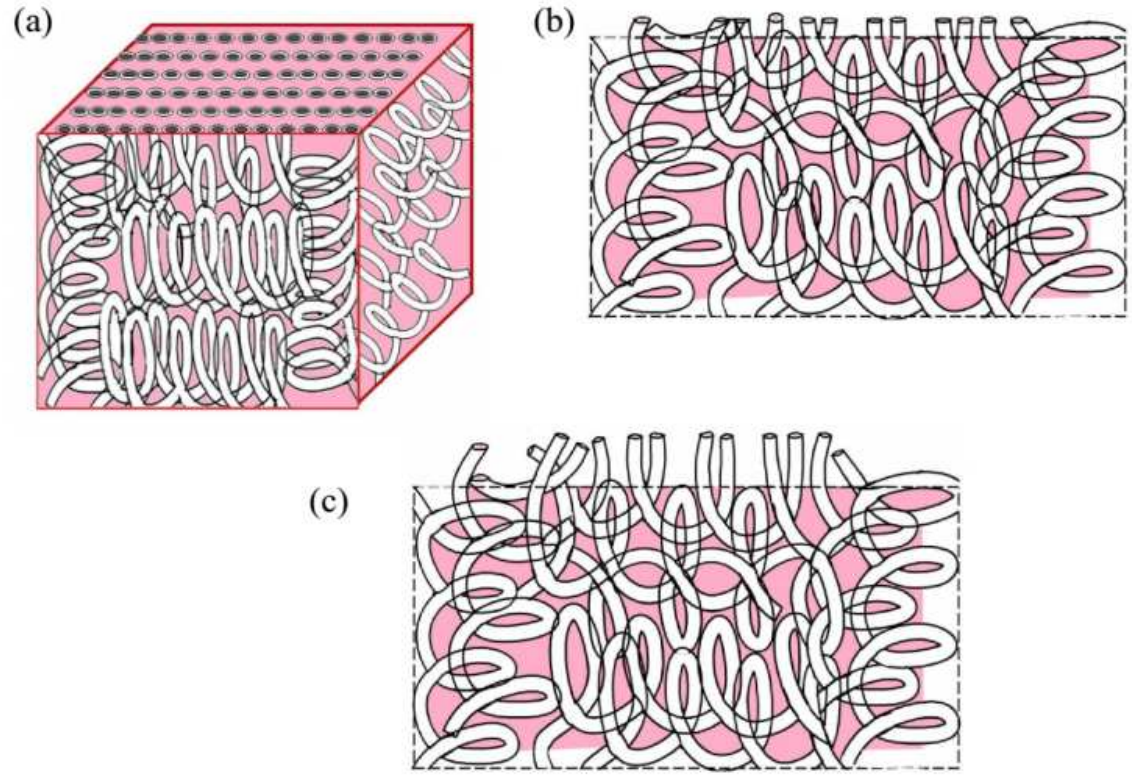

Fig. 3.

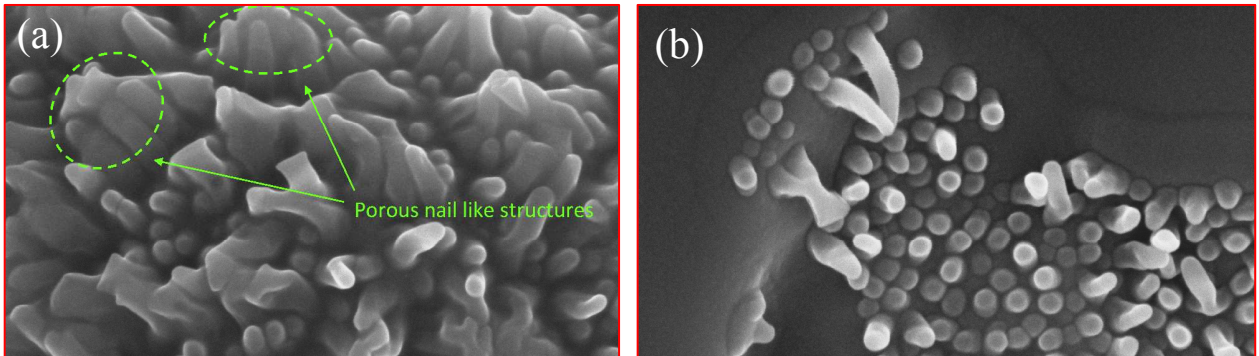

Fig. 4.

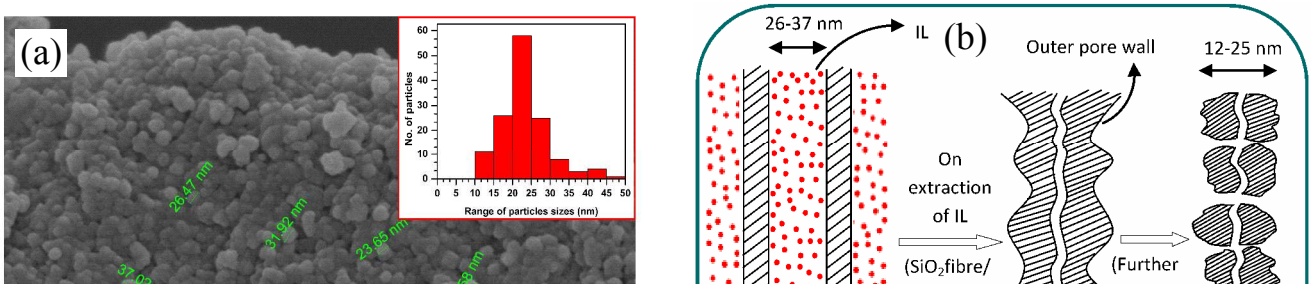

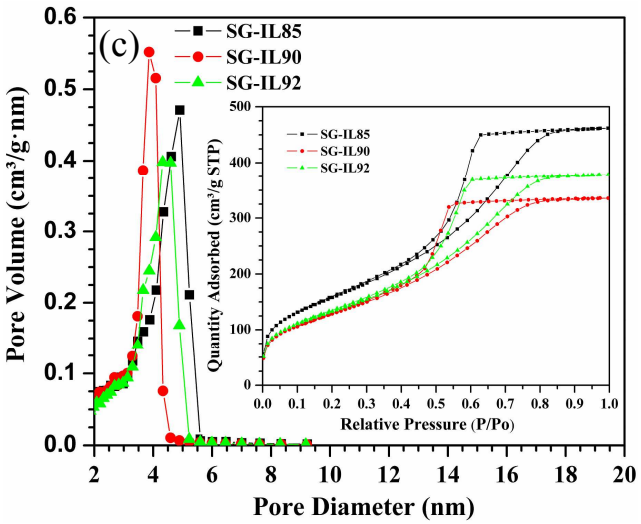

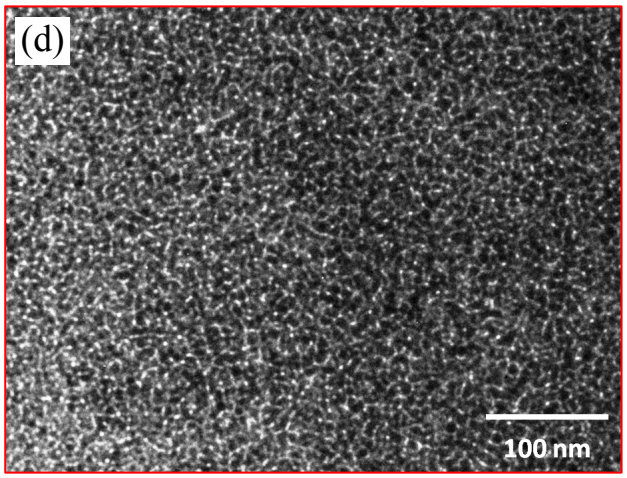

Fig.5.

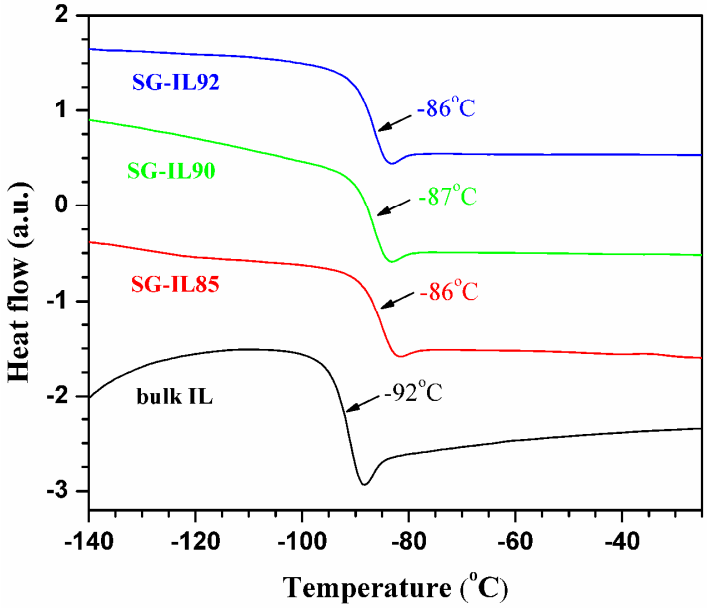

Fig.6.

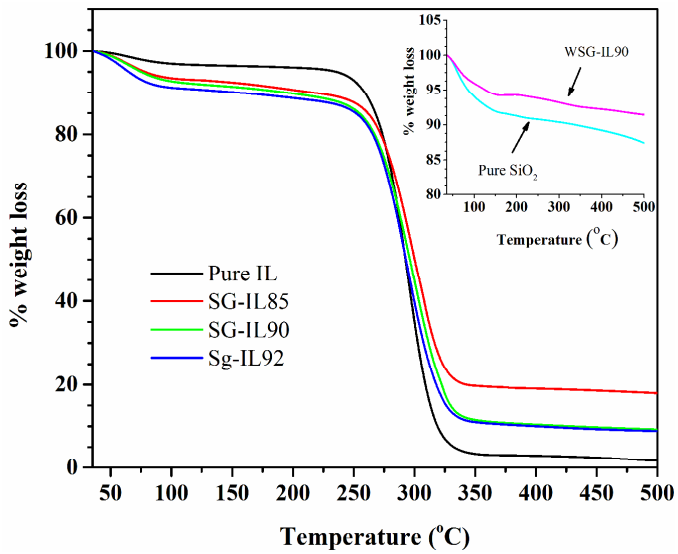

Fig.7.

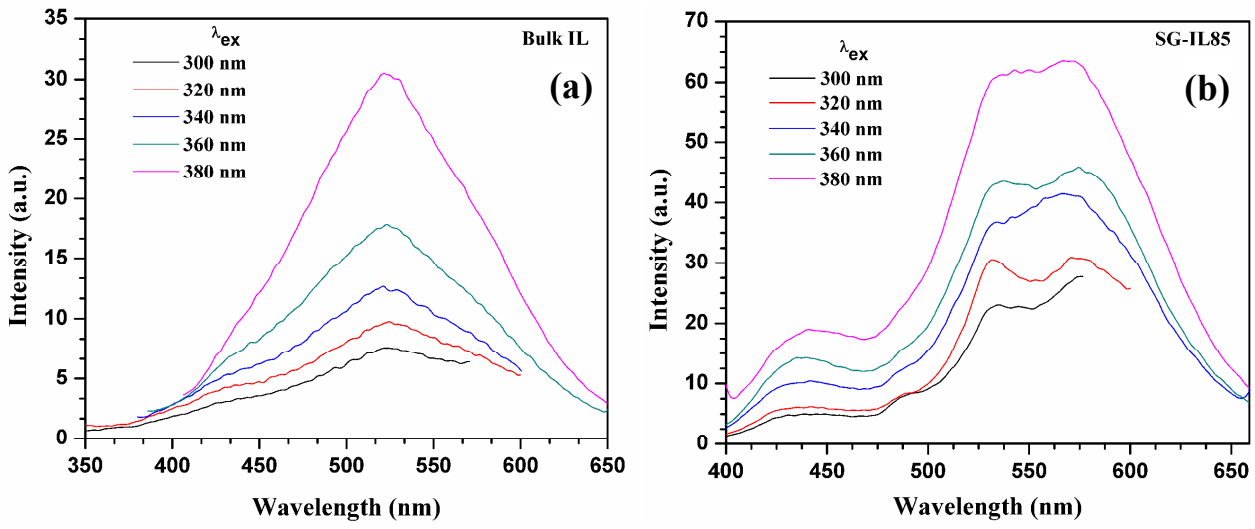

Fig.8.